Available online at www.sciencedirect.com
SCIENCE DIRECT®
Surface Science 521 (2002) 84–94
SURFACE SCIENCE
www.elsevier.com/locate/susc

Electron transfer and orbital hybridization in slow collisions between excited hydrogen atoms and aluminum surfaces

B. Bahrim [1], U. Thumm *

J.R. Macdonald Laboratory, Department of Physics, Kansas State University, Manhattan, KS 66506, USA

Received 10 June 2002; accepted for publication 6 September 2002

Abstract

We have developed a new two-center close-coupling approach in which the time-dependent Schrödinger equation is solved for an active electron interacting with a slow projectile and a metal surface. The motion of the active electron in the metal subspace is discretized by using Weyl wave packets. Results for the time evolution of the atomic and metallic population amplitudes for the H/Al system are shown and discussed.

Keywords: Atom–solid interactions; Hydrogen atom; Aluminum; Atomistic dynamics

1. Introduction

The detailed investigation of electron transfer and orbital hybridization in particle–surface interactions is of importance for several areas of applied physics and state-of-the-art technologies, such as sub-micro-scale electronics, the controlled modification and doping of materials with ion beams, sputtering, the development of ion sources, the control of ion–wall interactions in fusion plasma, and surface chemistry, including catalysis and corrosion prevention. In the past years, charge transfer during ion (atom)–solid surface collisions has received much interest, both experimentally and theoretically (for reviews see [1–4]). On the theoretical side, several non-perturbative methods have been developed. The method of complex coordinates [5] was applied to study hydrogen atoms, alkalis, and negative ions interacting with clean and adsorbate-covered surfaces [6–8]. The coupled-angular-modes method studies the scattering of the active electron by the atom-surface compound [9]. In this approach the perturbed atomic states appear as electron-scattering resonances. It has been applied to different atoms and ions interacting with clean surfaces [10] and surfaces covered by adsorbates [11]. The stabilization method has been used to study atomic resonances near an Al surface. It was implemented by using a multi-center Gaussian expansion [12] and in conjunction with the complex rotation technique [13].

* Corresponding author.
E-mail addresses: bahrimbm@hal.lamar.edu (B. Bahrim), thumm@phys.ksu.edu (U. Thumm).
[1] Current address: Department of Chemistry and Physics, Lamar University, P.O. Box 10046, Beaumont, TX 77710, USA.

0039-6028/02/$ - see front matter
PII: S0039-6028(02)02303-8

In the wave packet propagation method [14,15], the time evolution of the active electron's wave function is obtained by integrating the time-dependent Schrödinger equation on a numerical grid. This method has the advantage of being quite flexible with respect to the choice of effective potentials for the electron–atom and electron–surface interactions, but requires large computational resources for full three-dimensional calculations. Furthermore, a self-energy method has been applied [3,16–18] to the calculation of resonance widths and energies, by diagonalizing a complex Hamiltonian. In this method, the coupling of projectile levels to the surface conduction-band is approximately included in terms of the non-Hermitian "self-energy", which acts as a complex optical potential in the subspace spanned by the projectile-centered atomic bases states.

The aim of this paper is to apply a new close-coupling method for atom (ion)–surface interactions, which includes the electronic degrees of freedom inside the metal by using wave packets. Similar to the use of pseudo states obtained by representing the electronic continuum [19–22] in close-coupling calculations for charge exchange in ion–atom collisions or in the study of ionization phenomena, we use Weyl wave packets to discretize the continuum of bound conduction-band states of the metal surface. This wave packet approach takes couplings between metal states explicitly into account and allows for the evaluation of the population of both atomic and metal states [23,24].

Inherently, the scattering of atoms and ions from surfaces is a complex process that involves many-electrons. Such dynamical many-electron interactions constitute a major challenge to theory and are in our case further complicated by the need to discretize the conduction-band continuum. Rather than attempting to formulate and implement a many-electron description, we limit our theory to the motion of one electron as induced by an effective potential and assume excited $n = 2$ hydrogen atoms as projectiles that become ionized by the resonant loss of the active electron into the unoccupied part of the metal conduction-band. Previous non-perturbative calculations of the widths of H levels in both ground and excited states near an Al surface [14] have revealed transition rates between 1s and $n = 2$ excited states of H atoms and the conduction-band of Al, to be large at small ion-surface distances, with somewhat large rates for transitions into $n = 2$ levels (averaged over both hybrids). This means, that in the actual physical process during the reflection of excited hydrogen atoms from a Al surface two processes compete; electron loss to the conduction-band of the excited atomic electron and electron capture into the ground state of H.

Rather than aiming at comparisons with experiments, our main interest in this paper is to carefully investigate and eliminate convergence, coherence, and recurrence problems that usually accompany discretization schemes [18–20]. We therefore remain within the limits imposed by an effective potential, one-active-electron description of the charge transfer process and focus on the decay of an excited H state near an Al surface, thereby disregarding the competing neutralization into the projectile's ground state.

This paper is structured as follows. In Section 2, the close-coupling theory including continuum discretization is developed. In Section 3, we discuss numerical applications to the H/Al system. Our conclusions follow in Section 4. Throughout this paper, projectile-surface distances will be measured with respect to the jellium edge of the surface. The electronic energy reference will be the atomic ionization threshold. We use atomic units throughout.

2. Close-coupling theory with continuum discretization

2.1. Hamiltonian and channel splitting

The interaction scenario of a slowly moving atom and a metal surface is depicted schematically in Fig. 1. The reference frame is chosen at rest relative to the substrate such that the metal jellium edge coincides with the (x, y) plane. $z = 0$ defines the jellium plane. Oz is the quantization axis which passes through the center of the atom and is perpendicular to the surface plane, pointing away from surface. The vectors $\vec{r}$ and $\vec{r}_{\mathrm{p}}$ designate the

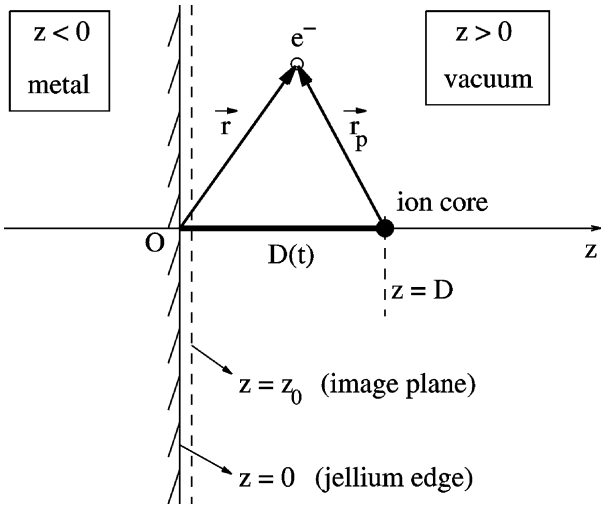

Fig. 1. Schematic diagram illustrating the interaction scenario between a projectile atom and a metal surface.

active electron with respect to the surface and projectile nucleus, respectively, and $D(t)$ is the projectile-surface distance, with $D = 0$ at the jellium edge. We assume perpendicular incidence of the projectile and use a classical trajectory given by $D(t) = d_{\min} \mp v_z t$ to describe its incidence and reflection at the surface. $d_{\min}$ is the distance of minimum approach to the jellium edge, and v_z is the perpendicular velocity of the projectile.

Our goal is to solve the time-dependent Schrödinger equation

$$H\psi(\vec{r},t) = i\frac{\partial\psi(\vec{r},t)}{\partial t} \tag{1}$$

as a system of differential coupled equations for the atomic and metallic population amplitudes, using a two-center expansion for the total wave function of the active electron.

In contrast to other close-coupling approaches [6,9,12,13,16–18], we discretize the active electron's motion inside the metal using Weyl wave packets [20,22,25]. These wave packets are obtained as the superposition of metal wave functions over small momentum intervals and, in contrast to metal conduction-band (e.g. jellium) states, have the advantage of being localized at the surface, where the electronic interactions occur. The use of discretized states to represent the conduction-band (and possibly the ionization) continuum allows for the convenient inclusion of (one-electron) inelastic processes inside the substrate.

The total Hamiltonian of the ion-surface system,

$$H = T + V_{\rm a} + V_{\rm surf}, \tag{2}$$

includes the kinetic energy of the active electron, T, the potential

$$V_{\rm a} = V_{\rm coul}\left(\Theta(z) + \Theta(-z)\mathrm{e}^{-\frac{|z|}{\lambda}}\right) \tag{3}$$

and the surface potential $V_{\rm surf}$. The potential $V_{\rm a}$ consists of the atomic Coulomb potential $V_{\rm coul} = -Q/r_{\rm p}$, exponentially screened at the jellium edge. Q designates the projectile nuclear charge, λ is the screening length inside the metal ($\lambda = 1$ for Al [26]), and $\Theta(z)$ is the unit step function. $V_{\rm surf}$ contains the step-potential $V_{\rm s} = -V_0\Theta(-z)$ and electronic and nuclear image potentials. The step-potential and the image potentials are matched at the distance $z_{\rm match} > 0$ in order to guarantee the continuity of the effective surface potential,

$$V_{\rm surf} = \begin{cases} -V_0 & z < z_{\rm match} \\ -\frac{1}{4(z-z_0)} + \frac{Q}{|D+z-2z_0|} & z > z_{\rm match} \end{cases} \tag{4}$$

at the surface. V_0 is the energy at the bottom of the conduction-band ($V_0 = 0.58$ for Al [16]). The nuclear image potential, $Q/|D+z-2z_0|$, has been approximated by its value on the surface normal through the projectile nucleus. The image-charge plane for the Al surface is located at $z_0 = 0.7$ [16].

We identify the initial and final asymptotic channel Hamiltonians as

$$H_{\rm i} = T + V_{\rm s} \tag{5}$$

and

$$H_{\rm f} = T + V_{\rm coul}. \tag{6}$$

The jellium wave functions $\phi_{\vec{k}}$ are eigenfunctions of the initial channel Hamiltonian, with energies E_k,

$$H_{\rm i}\phi_{\vec{k}} = E_k\phi_{\vec{k}}. \tag{7}$$

The projectile-centered hydrogenic wave functions ψ_j with energies E_j are eigenfunctions of the final channel Hamiltonian $H_{\rm f}$,

$$H_{\rm f}\psi_j = E_j\psi_j. \tag{8}$$

This identification is consistent with the channel decompositions of the total Hamiltonian,

$$H = H_i + V_i \tag{9}$$

and

$$H = H_f + V_f \tag{10}$$

with the perturbation potentials in the initial and final charge-transfer channels,

$$V_i = V_a + V_{surf}\Theta(z) \tag{11}$$

and

$$V_f = V_{coul}(e^{-\frac{|z|}{\lambda}} - 1)\Theta(-z) + V_{surf}. \tag{12}$$

2.2. Basis wave functions

We solve the time-dependent Schrödinger equation in adiabatic approximation by expanding the total wave function of the active electron as

$$\psi(\vec{r},t) = \sum_j a_j(t)e^{-iE_jt}\psi_j(\vec{r},D) + \int b_{\vec{k}}(t)e^{-iE_kt}\phi_{\vec{k}}(\vec{r})\rho_{\vec{k}}\,d\vec{k}, \tag{13}$$

where $\rho_{\vec{k}}$ is the metal density of states. Due to the cylindrical symmetry of the Hamiltonian, the projection of the electron orbital angular momentum m on the symmetry axis is a good quantum number, and atomic orbitals with different m do not couple.

The step-potential wave function corresponding to a given electron momentum $\vec{k} = (k_x, k_y, k_z)$ and energy

$$E_k = \frac{k_x^2}{2} + \frac{k_y^2}{2} + \frac{k_z^2}{2} - V_0 \tag{14}$$

is given by

$$\phi_{\vec{k}}(\vec{r}) = \frac{1}{(2\pi)^{3/2}}e^{ik_xx}e^{ik_yy}g_{k_z}(z), \tag{15}$$

where

$$g_{k_z}(z) = [e^{ik_zz} + R(k_z)e^{-ik_zz}]\theta(-z) + T(k_z)e^{-\gamma z}\theta(z). \tag{16}$$

$R(k_z)$ and $T(k_z)$ are the reflection and transmission coefficients [27], and $\gamma = \sqrt{2V_0 - k_z^2}$ characterizes the decrease of the wave function outside the metal.

We discretize the continuum of metal conduction-band states with energies between $-V_0$ and the ionization threshold by replacing the "metallic part" of the total electron wave function in (13) with a finite sum of Weyl wave packets. For $\Delta E_k t \ll \pi$, the exponential function e^{-iE_kt} in (13) is nearly independent of energy. For $r\Delta k \ll \pi$, the wave function $\phi_{\vec{k}}$ in (13) is nearly independent of momentum. In either case, the metallic part of the wave function may be replaced [25] by

$$\begin{aligned}
&\int b_{\vec{k}}(t)e^{-iE_kt}\phi_{\vec{k}}(\vec{r})\rho_{\vec{k}}\,d\vec{k} \\
&\quad\approx e^{iV_0t}\sum_p b_{\bar{k}_{xp}}(t)\frac{1}{\delta_x}\int_{\bar{k}_{xp}-\delta_x/2}^{\bar{k}_{xp}+\delta_x/2} e^{-iE_pt}\,dk_x \\
&\qquad\times\int_{\bar{k}_{xp}-\delta_x/2}^{\bar{k}_{xp}+\delta_x/2}\phi_{k_x}(x)\rho_{k_x}\,dk_x\sum_q b_{\bar{k}_{yq}}(t)\frac{1}{\delta_y} \\
&\qquad\times\int_{\bar{k}_{yq}-\delta_x/2}^{\bar{k}_{yq}+\delta_x/2} e^{-iE_qt}\,dk_y\int_{\bar{k}_{yq}-\delta_y/2}^{\bar{k}_{yq}+\delta_y/2}\phi_{k_y}(y)\rho_{k_y}\,dk_y \\
&\qquad\times\sum_i b_{\bar{k}_{zi}}(t)\frac{1}{\delta_z}\int_{\bar{k}_{zi}-\delta_x/2}^{\bar{k}_{zi}+\delta_x/2} e^{-iE_it}\,dk_z\int_{\bar{k}_{zi}-\delta_z/2}^{\bar{k}_{zi}+\delta_z/2}\phi_{k_z}(z)\rho_{k_z}\,dk_z \\
&\quad= \sum_\mu b_\mu(t)e^{-iE_\mu t}\phi_\mu(\vec{r}),
\end{aligned} \tag{17}$$

where $\mu = (p,q,i)$ labels wave packets in Ox, Oy, and Oz directions, and $E_\mu = E_p + E_q + E_i - V_0$. The wave functions $\phi_{\vec{k}}$ are normalized to $\delta(\vec{k} - \vec{k}')$, and the density of states $\rho_{\vec{k}} = \rho_{k_x}\rho_{k_y}\rho_{k_z}$ is taken equal to unity. δ_x, δ_y, and δ_z are small momentum intervals, corresponding to the momentum discretization of $\phi_{\vec{k}}$ in Ox, Oy, and Oz directions. In using the approximation (17), we are aware of possible dephasing effects in time, and distance. They may appear whenever the conditions $\Delta E_k t \ll \pi$ or $r\Delta k \ll \pi$ are violated. For $t \leqslant \pi/\Delta E_k$, the wave functions ϕ_k with different k inside the integration intervals in (17) will get dephased by the quantal phases e^{-iE_kt}. Similarly, when the distance traveled by the projectile exceeds the estimate obtained from the condition $r\Delta k \ll \pi$, dephasing occurs due to the exponentials e^{ikr} in the spacial part of ϕ_k. In order to eliminate dephasing effects in our calculations, we use sufficiently small momentum intervals. These effects are discussed in more detail in Section 3.

For the electron motion along the surface normal, wave packets are obtained by superimposing jellium wave functions within the small interval δ_z about the centroid momentum $\bar{k}_{z_i}$,

$$\phi_{\bar{k}_{z_i}}(z) = \sqrt{\frac{\delta_z}{2\pi}} \frac{2\sin(\frac{\delta_z z}{2})}{\delta_z z} g_{\bar{k}_z}(z), \tag{18}$$

where the reflection and transmission coefficients, R and T, and the decay parameter γ are evaluated at the centroid momentum $\bar{k}_{z_i}$ and are assumed to be independent of k_z inside the interval $[\bar{k}_{z_i} - \delta_z/2, \bar{k}_{z_i} + \delta_z/2]$.

For the motion in the surface plane, wave packets are obtained by superimposing plane waves within small intervals δ_x and δ_y about the centroid momenta $\bar{k}_{x_p}$ and $\bar{k}_{y_q}$, respectively,

$$\phi_{\bar{k}_{x_p}}(x) = \sqrt{\frac{\delta_x}{2\pi}} \frac{2\sin(\frac{\delta_x x}{2})}{\delta_x x} \mathrm{e}^{\mathrm{i}\bar{k}_{x_p} x}, \tag{19}$$

$$\phi_{\bar{k}_{y_q}}(y) = \sqrt{\frac{\delta_y}{2\pi}} \frac{2\sin(\frac{\delta_y y}{2})}{\delta_y y} \mathrm{e}^{\mathrm{i}\bar{k}_{y_q} y}. \tag{20}$$

The wave functions ($\phi_{\bar{k}_{x_p}}$,$\phi_{\bar{k}_{y_q}}$, $\phi_{\bar{k}_{z_i}}$) are orthonormal. They are localized near and in the surface and near the Oz symmetry axis due to the damping factors $(2\sin(\delta_\xi \xi/2))/(\delta_\xi \xi)$, $\xi = x, y, z$. The spatial extent of the wave function envelope is proportional to the inverse of the interval lengths δ_x, δ_y, and δ_z. This localization of the Weyl wave packet introduces a "soft boundary" at which electronic probability density might be reflected, possibly giving rise to recurrence effects. These effects will be discussed in Section 3.1.

2.3. System of coupled equations

Insertion into Eq. (1) of the expansion (13) with the metal part (17) leads to the system of coupled equations for the amplitudes $a_j(t)$ and $b_\mu(t)$,

$$\begin{aligned} i \begin{pmatrix} 1 & : & \langle\psi_j|\phi_\mu\rangle \\ \cdots & \cdot & \cdots \\ \langle\phi_\mu|\psi_j\rangle & : & 1 \end{pmatrix} \begin{pmatrix} \mathrm{e}^{-\mathrm{i}E_j t} & : & 0 \\ \cdots & \cdot & \cdots \\ 0 & : & \mathrm{e}^{-\mathrm{i}E_\mu t} \end{pmatrix} \begin{pmatrix} \dot{a}_j(t) \\ \cdot \\ \dot{b}_\mu(t) \end{pmatrix} \\ = \begin{pmatrix} \langle\psi_j|V_\mathrm{f}|\psi_{j'}\rangle & : & \langle\psi_j|V_\mathrm{i}|\phi_\mu\rangle \\ \cdots & \cdot & \cdots \\ \langle\phi_\mu|V_\mathrm{f}|\psi_j\rangle & : & \langle\phi_\mu|V_\mathrm{i}|\phi_{\mu'}\rangle \end{pmatrix} \\ \times \begin{pmatrix} \mathrm{e}^{-\mathrm{i}E_j t} & : & 0 \\ \cdots & \cdot & \cdots \\ 0 & : & \mathrm{e}^{-\mathrm{i}E_\mu t} \end{pmatrix} \begin{pmatrix} a_j(t) \\ \cdot \\ b_\mu(t) \end{pmatrix}. \end{aligned} \tag{21}$$

The elements $\langle\psi_j|\phi_\mu\rangle$ are the overlaps between the atomic and metal wave functions. The coupling matrix contains interaction matrix elements between atomic and metal states, $\langle\psi_j|V_\mathrm{i}|\phi_\mu\rangle$ and $\langle\phi_\mu|V_\mathrm{f}|\psi_j\rangle$, and elements $\langle\phi_\mu|V_\mathrm{i}|\phi_{\mu'}\rangle$ which describe the direct couplings between wave packets by the initial channel perturbation V_i. Since we study slow ion–surface collisions, translation factors are neglected in Eq. (21).

The system of close-coupled equations is integrated using a Runge–Kutta procedure with adaptive step size [28]. Thus, for a given initial occupation, we can calculate the time-dependence of atomic and metal occupation amplitudes, $a_j(t)$ and $b_\mu(t)$, over the whole collision trajectory.

3. Results

3.1. Results for $k_\parallel \approx 0$

We designate the numbers of wave packets used to represent the motion of metal electrons in the surface plane and along the surface normal with $N_\parallel$ and $N_\perp$, respectively. N_A denotes the number of projectile-centered hydrogenic orbitals in our close-coupling expansion. In order to limit the computational effort in our numerical applications and to understand the basic processes occurring in the collision, we first disregard the active electron's motion in the surface plane by assuming $k_\parallel = \sqrt{k_x^2 + k_y^2} \approx 0$. In the sums over p and q in (17), we expect dominant contributions from metal electrons with parallel momenta contained in a small interval around $k_\parallel = 0$, due to relatively large transmission coefficients T. Therefore, we restrict the expansion (17) to conduction-band electrons contained in a narrow cylinder of diameter $\delta_\parallel$ centered at $k_\parallel = 0$ inside a sphere of radius $k_\mathrm{max} = \sqrt{2V_0} = 1.077$. For $\delta_\parallel = 0.02$, a numerical study has shown that all transfer matrix elements with $|k_\parallel| \leqslant \delta_\parallel$ are approximately constant in $k_\parallel$ (their magnitude varies by less than 0.1%).

We study a hydrogen atom initially excited to the $2p_0$ level at perpendicular incidence on an aluminum surface with speed $v_z = 0.02$. The quantization axis is oriented along the surface normal. We first focus our attention on the excited 2s and

$2p_0$ levels of hydrogen which are resonantly coupled to the empty conduction-band continuum of aluminum. In order to study hybridization effects, we investigated the occupation evolution in the ($n = 2$, $m = 0$) manifold in spherical (2s and $2p_0$) and parabolic (electric quantum numbers $k = \pm 1$) representations. The atom–surface interaction is represented in terms of a planar averaged Thomas–Fermi–Molière potential energy [29], from which we obtain the distance of closest approach (to the jellium edge) $d_{\min} = 0.5$.

For all results presented in this section, we have carefully investigated:

(1) the convergence with respect to the number of wave packets needed to describe the conduction-band continuum,
(2) possible dephasing effects in distance and time,
(3) possible recurrence effects due to the use of a discrete basis set to represent the metal continuum.

All results in this subsection are obtained by close-coupling the 1s, 2s, and $2p_0$ projectile states with 200 metal Weyl packets ($N_\perp = 200$, $N_\parallel = 1$, and $N_A = 3$) and are converged with respect to the number ($N_\perp = N_{\perp,1} + N_{\perp,2}$) of included Weyl packets $\phi_{\bar{k}_{z_i}}$. We choose a higher density of wave-packets in the momentum interval $[0.75 - k_{\max}]$ ($N_{\perp,1} = 180$ packets), since this interval includes the metal continuum in resonance with the projectile levels, while a much smaller number of packets is sufficient to describe the [0–0.75] momentum interval ($N_{\perp,2} = 20$ packets). Thus, the packets in resonance with the atomic states (with $n \geqslant 2$) will have a smaller width ($\delta_z = 0.0036$ a.u. of momentum) than the packets outside the resonance region ($\delta_z = 0.075$ a.u.).

Even though we obtained converged results with $N_\perp = 80$ Weyl packets, we prefer to use $N_\perp = 200$ packets in order to better justify the approximation in Eq. (17), of factorizing the integral of the metallic wave function over momentum in two parts (see Section 2.2.). In order to address possible dephasing effects, we focus on momentum states with $|\vec{k}| \approx 1$. No dephasing occurs over the integration distance r, if $\Delta k \ll \pi/r$. In our calculations, $r \approx 100$, and the condition $\Delta k \ll 0.431$ from the above estimate is fulfilled, since $\Delta k = \delta_z = 0.0036$. With regard to the population evolution of the $n = 2$ atomic manifold, relevant charge transfer processes take place within 7–8 a.u. in front of the surface, which translates into an interaction time of about 700. Therefore, dephasing in time is expected to occur at about 700 a.u. in time after the beginning of charge transfer. Our current computing facilities do not allow us to significantly increase the number of metal wave packets, in order to strictly comply with the condition $t \ll \pi/\Delta E_k$. However, for a total interaction time below 700 a.u., dephasing at later times does not influence the evolution of atomic probability amplitudes.

Fig. 2 shows results for a calculation with the atomic levels 1s, 2s, and $2p_0$ in Eq. (17). The 1s projectile state does not couple significantly to the metal or other projectile states during the collision. The squared amplitudes $|a_j|^2$ corresponding to 2s and $2p_0$ levels and to the sum of all metal states $\sum_\mu |b_\mu|^2$ are shown as a function of $D - d_{\min}$. Initially, the $2p_0$ level is occupied and the 1s (not shown) and 2s levels are empty. On the incoming trajectory, two different regions can be distinguished. For ion-surface distances D larger than

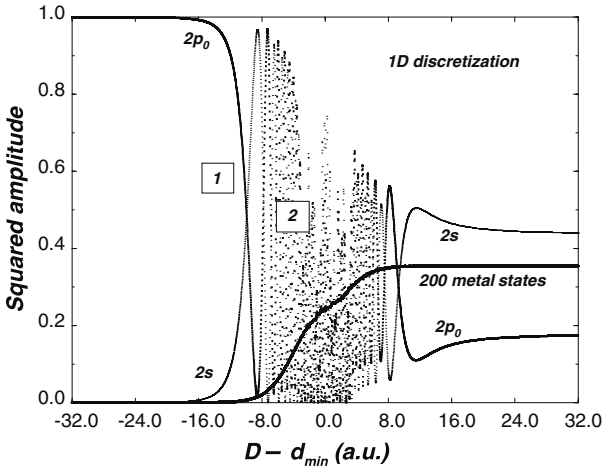

Fig. 2. 2s and $2p_0$ levels of hydrogen interacting with an aluminum surface at perpendicular incidence with speed $v_z = 0.02$ a.u., in spherical representation. The aluminum conduction-band continuum is discretized by using 200 Weyl wave packets ($N_\perp = 200$, $N_\parallel = 1$, $N_A = 3$). Squared amplitudes as a function of the distance $D - d_{\min}$ from the projectile turning point.

10.5 (or $D - d_{\min} = 10$), "Stark-like" mixing between the two states occurs due to the interaction with the surface (region $\boxed{1}$ in the figure). The electron is "shared" (hybridized) between 2s and $2p_0$ levels, but there is no charge exchange with the metal subspace. Below $D - d_{\min} = 10$, in the second region (labeled by $\boxed{2}$), the 2s and $2p_0$ atomic levels strongly mix and begin to decay into the metal, as is seen by the increasing population density of the metal subspace. At large atom-surface distances on the outgoing trajectory, the atomic and metal amplitudes stabilize to constant values which yield the final atomic and metal occupations after the collision.

These results are free of recurrence effect. We have investigated possible recurrence effects for this calculation in the following way. We have compared the collision time for $v_z = 0.02$ with the recurrence time for an electron initially in the $2p_0$ state that interacts with a continuum described by 200 packets. In order to estimate the recurrence time, we keep the projectile fixed at a small distance, 5 a.u., in front of the surface. Fig. 3 shows the net probability density in the atomic $2p_0$ level as a function of time. The simple exponential decay of the atomic probability density into the substrate rules out recurrence effects in the atomic population up to over 4000 a.u. in time, after which the atomic level is almost depleted. The collision time is much smaller, and estimated roughly as being $2(D - d_{\min})/v_z = 500$, where

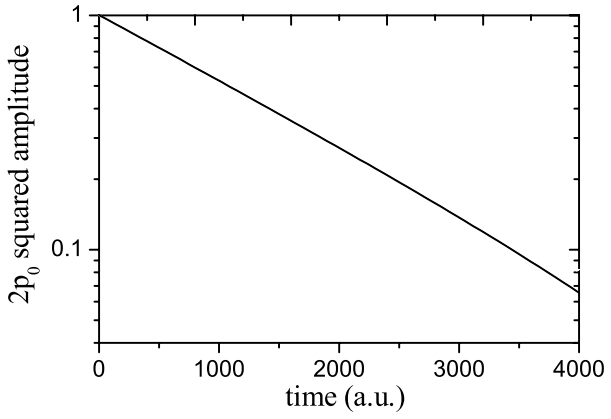

Fig. 3. Decay of the $2p_0$ level of a hydrogen atom at a fixed atom-surface distance of 5 a.u. The 1D calculation includes 200 Weyl wave packets. Squared amplitude as a function of time.

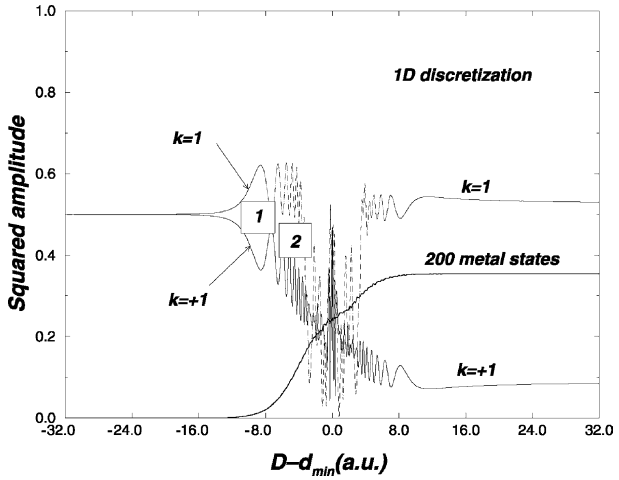

Fig. 4. Same as Fig. 2, but in parabolic representation of the projectile orbitals. Electric quantum numbers $k = -1$ and 1 correspond to orbitals oriented away from and toward the surface.

$D - d_{\min} \approx 5$ is the distance where significant charge exchange with the metal starts.

Fig. 4 shows the results of Fig. 2 in parabolic representation of the hydrogen states [30]. The population in the parabolic states with electric quantum numbers $k = -1$ and $+1$ varies less during the collision than the 2s and $2p_0$ occupations in Fig. 2, indicating that a significant part of the hybridization near a metal surface corresponds to the Stark-like mixing of spherical hydrogenic states in the electric field of the surface [18]. For this reason the parabolic representation is more appropriate than the spherical representation. The $k = -1$ orbital points away from surface. Due to the smaller overlap with the surface, its coupling to the surface conduction-band is weaker than for the $k = +1$ orbital (which points toward the surface) and results in a smaller charge transfer to the metal half space. As for the spherical representation in Fig. 2, Fig. 4 shows that surface-induced mixing of the projectile states prevails in region $\boxed{1}$, without transfer to the metal. Charge transfer is restricted to the smaller distances in region $\boxed{2}$.

In order to study the convergence of our results with respect to the number of atomic states, N_A, introduced in the calculation, we present in Fig. 5 the final population of the initially occupied $2p_0$ level and of the 2s level for calculations in which

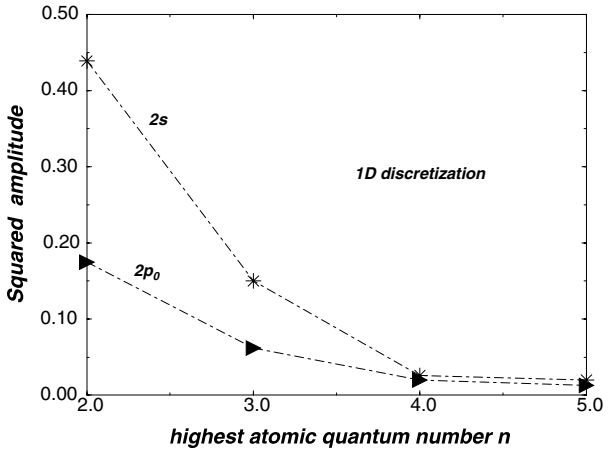

Fig. 5. Convergence study for the $2p_0$ and 2s level populations as a function of the number, $3 \leqslant N_A \leqslant 15$, of atomic manifolds included in the calculation.

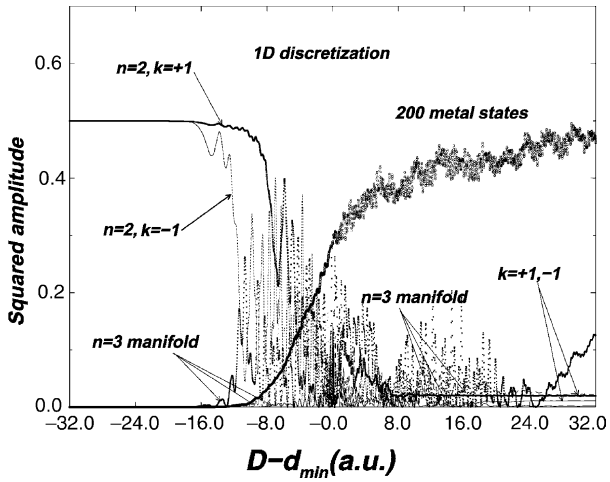

Fig. 6. Time evolution of squared amplitudes for the $n = 2$ and 3 manifolds and all 200 Weyl packets used to discretize the metal continuum, in parabolic representation. The calculation includes all ($n \leqslant 5$, $m = 0$) atomic basis states ($N_\perp = 200$, $N_\parallel = 1$, $N_A = 15$). Same collision system and speed as in Fig. 2.

the ($n \leqslant 2$, $m = 0$), ($n \leqslant 3$, $m = 0$), ($n \leqslant 4$, $m = 0$), and ($n \leqslant 5$, $m = 0$) atomic manifolds, i.e., $N_A = 3$, 6, 10, and 15 levels, are included in the calculation. The results including the $n > 2$ levels are different from the ones that only include the $n = 2$ manifold. Since the results with $n \leqslant 4$ and $n \leqslant 5$ are comparable, we assume that our results are converged if all ($n \leqslant 5$, $m = 0$) projectile levels are included.

Fig. 6 shows the evolution of all ($n = 2$, $m = 0$) and ($n = 3$, $m = 0$) squared amplitudes in parabolic representation, for a calculations with all levels ($n \leqslant 5$, $m = 0$) projectile levels ($N_\perp = 200$, $N_\parallel = 1$, $N_A = 15$). At $D - d_{min} = 15.5$ on the incoming trajectory, the $n = 3$ manifold becomes populated from the initially occupied $2p_0$ level, hindering in this way $2p_0$ and 2s levels from pure Stark mixing. Electron transfer into the metal starts at $D \approx 12.5$ ($D - d_{min} \approx 12$), i.e., at a distance between the classical threshold distances for over-barrier capture $D_{n=2} = 8$ and $D_{n=3} = 18$ [31]. On the outgoing trajectory, the population of $k = -1$ and $+1$ components is stable and very small, while surface-induced level mixing inside the $n = 3$ manifold and interactions with higher projectile manifolds continue to change the populations in the ($n = 3$, $m = 0$) subspace at $D - d_{min} > 32$. The structure at $D - d_{min} = 32$ in the $n = 3$ population is due mainly to the interaction with the $n = 4$ manifold.

3.2. Results for $k_\parallel \neq 0$

We first investigate the influence of different parallel electron momenta $\vec{k}_\parallel$, chosen along an arbitrary direction in the surface plane, on the population evolution of a particular set of atomic states. Due to the cylindrical symmetry and for magnetic quantum numbers $m = 0$, all matrix elements are invariant under rotations about the Oz axis in $\vec{k}$ space. Wave packets in the parallel direction are constructed according to (19) with parallel momenta contained in small cylindrical shells of thickness $\delta_\parallel = 0.01$ such that $|\vec{k}| = \sqrt{k_\parallel^2 + k_z^2} \leqslant k_{max}$ (see Fig. 7).

Fig. 8 presents results for separates calculations for incident excited hydrogen atoms initially in the $3s$ or $2p_0$ state ($N_A = 1$). The aluminum surface is described by $N_\perp = 10$, 16, or 40 metal wave packets in the Oz direction and a variable number $N_\parallel$ of Weyl packets in the $k_\parallel$ direction. In successive calculations, we included more and more metal wave packets of the form (19) with increasing $k_\parallel$ values, and studied the influence on the final atomic populations after the collision. Thus, the first point on each curve in Fig. 8 corresponds to a calculation in which the electronic motion in the surface plane is represented by one wave packet

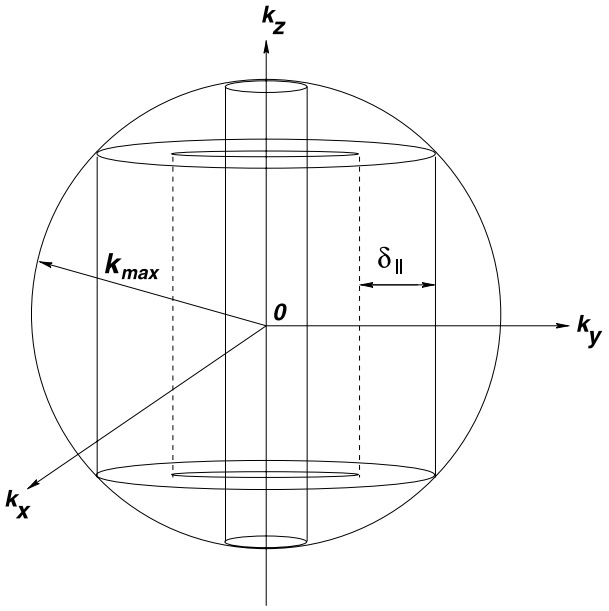

Fig. 7. Momentum discretization in parallel direction in cylindrical coordinates.

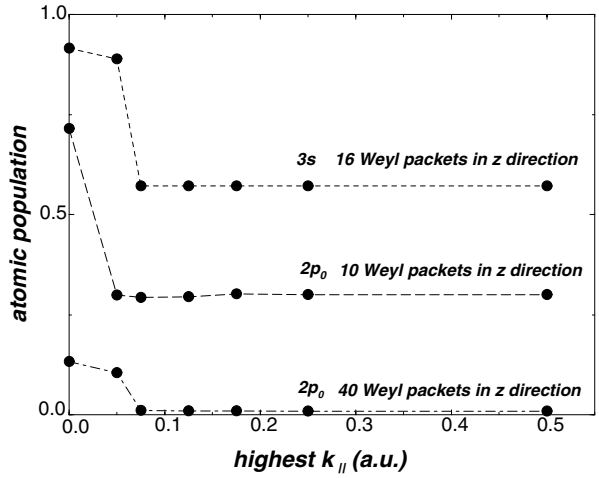

Fig. 8. Convergence study of the final atomic population after the collision, as a function of the highest parallel momentum of the number $N_\parallel$ of wave packets used to represent the electronic motion in the surface plane. Upper curve: $N_\perp = 16$, $N_A = 1$; middle curve: $N_\perp = 10$, $N_A = 1$; lower curve: $N_\perp = 40$, $N_A = 1$. The projectile is initially in the 3*s* state (upper curve) or in the $2p_0$ state (middle and lower curve).

($N_\parallel = 1$) with $k_\parallel = 0$ only. The second point on each curve corresponds to a calculation in which $k_\parallel = 0$ and 0.05 are included ($N_\parallel = 2$), and the last point on each curve corresponds to a calculation in which all parallel momenta indicated by the symbols, up to $k_\parallel = 0.5$, are included ($N_\parallel = 7$).

These results show that the momentum region which affects the final populations most is $|\vec{k}_\parallel| \leqslant 0.075$. Therefore, the assumption in Section 3.1., that the main contribution in the sums over p and q in (17) comes from metal electrons with parallel momenta contained in a small region around $k_\parallel = 0$, is justified. These numerical tests suggest that it is sufficient to represent the $\vec{k}_\parallel$ plane by a rather small number of parallel momenta chosen in this particular interval of $k_\parallel$ values, in order to obtain final atomic populations that are converged with respect to the number of included metal wave packets.

We have seen that calculations with $N_\perp = 80$ wave packets in the direction perpendicular to the surface (see discussion in Section 3.1.), and $N_\parallel = 6$ wave packets in the $k_\parallel$ direction give converged results. This amounts to $N_\perp N_\parallel = 480$ wave packets in total for the two-dimensional (2D) discretization (in k_z and $k_\parallel$ directions).

In Fig. 9, the resulting metal occupation evolution obtained with the 2D discretization using all ($n \leqslant 3$, $m = 0$) atomic states and 480 metal wave packets is compared to the metal occupation obtained from a one-dimensional (1D) discretization

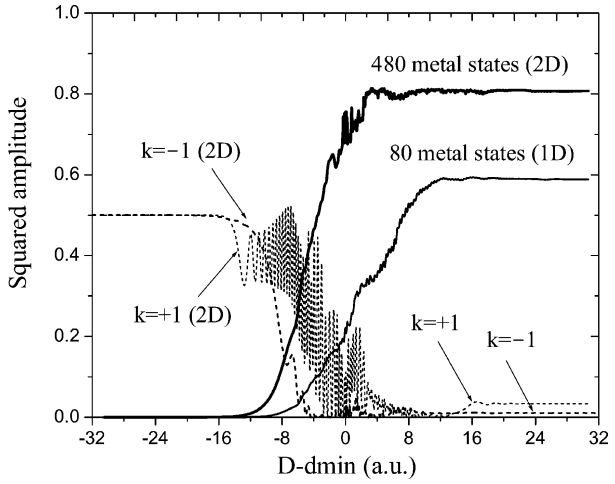

Fig. 9. Time evolution of squared amplitudes for the $n = 2$ manifold and the metal for 2D discretization ($N_\perp = 80$, $N_\parallel = 6$, $N_A = 6$), and for the metal only in a 1D calculation ($N_\perp = 80$, $N_\parallel = 1$, $N_A = 6$).

with all ($n \leqslant 3$, $m = 0$) ($N_A = 6$) atomic states and $N_\perp = 80$ metal wave packets. For the 1D calculation, we assume $k_\parallel = 0$. The $k = -1$ and $+1$ Stark states obtained with the 2D discretization are also indicated in the figure. For the 2D calculation, charge transfer to the metal surface starts earlier on the incoming trajectory as compared to the 1D result. In this particular case it starts at $D \approx 16.5$ (or $D - d_{\min} \approx 16$). As expected, we also notice a much faster decay for both $k = -1$ and $+1$ Stark states into the metal compared with the 1D result, due to the inclusion of many more states in the surface plane for the active electron to dissipate into. The final metal population after the collision for the calculation with 480 wave packets is higher than for the 1D result, in agreement with the expected increased possibility for dissipation.

We have investigated possible recurrence effects for the 2D calculation by comparing the collision time for $v_z = 0.02$ with the recurrence time of an electron in the $2p_0$ state interacting with a continuum described by 480 Weyl packets ($N_\perp = 80$, $N_\parallel = 6$). As in Section 3.1., we have estimated the recurrence time for the decay of a $2p_0$ level at a small fixed ion-surface distance of 5. The collision time $2(D - d_{\min})/v_z = 1000$ (for $D - d_{\min} \approx 10$) is smaller than the recurrence time of 3600, obtained from our calculations. So, recurrence exists, but does not affect our results. After being reflected on the soft boundary on the back side of the effective metal volume, the active electron does not continue to interact with the projectile. The rapid oscillations in the metal population near the turning point are due to the strong overlap between atomic and metal states, and are not due to recurrence effects. A separate calculation in which all wave function overlap terms were neglected produced monotonously increasing metal occupations without rapid oscillations.

4. Summary and outlook

We have developed a two-center close-coupling approach including the discretization of a metal conduction-band continuum for slow ion–surface interactions. In our method, the electronic motion inside the metal is fully discretized in terms of Weyl wave packets. The wave packet description explicitly takes into account electronic couplings inside the metal and evaluates the population of both atomic and metal states. In our numerical applications to H/Al collisions, we calculated the evolution of the atomic and metallic population amplitudes and discussed the main processes occurring during the collision. With access to faster computers, we hope to soon be able to completely eliminate possible remaining dephasing effects in time from our calculations. Our approach includes target inelastic processes in terms of single electron excitations (electron–hole pair creation). In addition, in future applications, our close-coupling method can be extended to include collective excitations of the surface by adding appropriate effective potentials for the active electron coupling to plasmons and phonons.

Acknowledgements

This work was supported by NSF grant PHY-9604872. We also acknowledge partial support by the Division of Chemical Sciences, Office of Basic Energy Sciences, Office of Energy Research, US DOE.

References

[1] J.J.C. Geerlings, J. Los, Phys. Rep. 190 (1990) 133.
[2] R.E. Palmer, P.J. Rous, Rev. Mod. Phys. 64 (1992) 383.
[3] J. Burgdörfer, in: C.D. Lin (Ed.), Review of Fundamental Processes and Applications of Atoms and Ions, World Scientific, Singapore, 1993, p. 517.
[4] J.P. Gauyacq, A. Borisov, D. Teillet-Billy, Formation/destruction of negative ions in heavy particle–surface collisions, in: V. Esaulov (Ed.), Negative Ions, Cambridge University Press, 1996.
[5] B.R. Junker, Adv. At. Mol. Phys. 18 (1982) 207.
[6] P. Nordlander, J.C. Tully, Phys. Rev. B 42 (1990) 5564.
[7] P. Nordlander, N.D. Lang, Phys. Rev. B 44 (1991) 13681.
[8] P. Nordlander, Phys. Rev. B 46 (1992) 2584.
[9] D. Teillet-Billy, J.P. Gauyacq, Surf. Sci. 239 (1990) 343.
[10] A. Borisov, D. Teillet-Billy, J.P. Gauyacq, Surf. Sci. 278 (1992) 99;
B. Bahrim, D. Teillet-Billy, J.P. Gauyacq, Phys. Rev. B 50 (1994) 7860.

[11] B. Bahrim, D. Teillet-Billy, J.P. Gauyacq, Surf. Sci. 431 (1999) 193.
[12] F. Martin, M.F. Politis, Surf. Sci. 356 (1996) 247.
[13] S.A. Deutscher, X. Yang, J. Burgdörfer, Nucl. Instrum. Meth. Phys. Res. B 100 (1995) 336.
[14] A.G. Borisov, A.K. Kazansky, J.P. Gauyacq, Phys. Rev. B 59 (1999) 10935.
[15] U. Thumm, in: Ion–Surface Interactions, Book of Invited Papers. XXII International Conference on Physics of Electronic and Atomic Collisions, Santa Fe, NM, Rinton Press, 2002, pp. 592–603.
[16] P. Kürpick, U. Thumm, U. Wille, Phys. Rev. A 56 (1997) 543.
[17] P. Kürpick, U. Thumm, U. Wille, Phys. Rev. A 57 (1998) 1920.
[18] P. Kürpick, U. Thumm, Phys. Rev. A 58 (1998) 2174.
[19] B.H. Bransden, M.R.C. McDowell, Charge Exchange and the Theory of Ion–Atom Collisions, Clarendon Press, Oxford, 1992.
[20] J.F. Reading, A.L. Ford, G.L. Swafford, A. Fitchard, Phys. Rev. A 20 (1979) 130.
[21] D.A. Micha, R.D. Piacentini, Phys. Rev. A 25 (1982) 204.
[22] H.J. Bär, G. Soff, Physica 128c (1985) 225.
[23] B. Bahrim, U. Thumm, Surf. Sci. 451 (2000) 1.
[24] B. Bahrim, P. Kürpick, U. Thumm, U. Wille, Nucl. Instrum. Meth. Phys. Res. B 164–165 (2000) 614.
[25] G. Schiwietz, Phys. Rev. A 42 (1990) 296.
[26] C. Kittel, in: Introduction to Solid State Physics, John Wiley and Sons Inc., New York, London, Sydney, 1968.
[27] U. Wille, Phys. Rev. A 45 (1992) 3004.
[28] R.W. Brankin, I. Gladwell, L.F. Shampine, RKSUITE: a suite of Runge–Kutta codes for the initial value problem for ODE's, Softreport 92-S 1, Department of Mathematics, Southern Methodist University, Dallas, Texas, USA, unpublished.
[29] J.J. Ducrée, F. Casali, U. Thumm, Phys. Rev. A 57 (1998) 338.
[30] U. Thumm, P. Kürpick, U. Wille, Phys. Rev. B 61 (2000) 3067;
D. Park, Z. Phys. 159 (1960) 155.
[31] U. Wille, Phys. Rev. B 50 (1994) 1888.